Bioinspired Hierarchical Designs for Stiff, Strong Interfaces between Materials of Differing Stiffness

Daniel Rayneau-Kirkhope,[1,2,*] Yong Mao,[3] and Cyril Rauch[4]

[1] *Aalto Science Institute, School of Science, Aalto University, 02150 Espoo, Finland*
[2] *Department of Applied Physics, Aalto University, 02150 Espoo, Finland*
[3] *School of Physics and Astronomy, University of Nottingham, Nottingham, NG7 2RD, United Kingdom*
[4] *School of Veterinary Medicine and Science, University of Nottingham, Sutton Bonington, LE12 5RD, United Kingdom*

(Received 4 August 2016; published 10 September 2018)

Throughout biology, geometric hierarchy is a recurrent theme in structures where strength is achieved with efficient use of material. Acting over vast timescales, evolution has brought about beautiful solutions to problems in mechanics that are only now being understood and incorporated into engineering designs. One particular example of structural hierarchy is found in the junction between stiff keratinized material and the soft biological matter within the hooves of ungulates. Using this biological interface as a design motif, we investigate the role of hierarchy in the creation of a stiff, robust interface between two materials. We show that through hierarchical design, we can manipulate the scaling laws relating constituent-material stiffness and overall interface stiffness under loading. Furthermore, we demonstrate that through use of a hierarchical geometry, we can reduce the maximum stress the materials experience for a given loading and tailor the ratio of maximum stresses in the constituent materials. We demonstrate that when two materials of different stiffness are joined, hierarchical geometries are linked with beneficial mechanical properties and enhanced tailorability of mechanical response.

DOI: 10.1103/PhysRevApplied.10.034016

I. INTRODUCTION

Naturally occurring hierarchical interfaces for adhesion between two surfaces have been well documented, and examples of such designs are to be found on the feet of geckos, spiders, and insects [1–3]. Although other contributions have been identified [4], it is understood that the primary interaction allowing geckos to walk up walls is the van der Waals interaction [5,6]. The hierarchical geometry of the gecko's foot is key in making this adhesion possible with use of this very weak interaction [7]. This structure has inspired a research area with the goal of creating dry adhesive mechanisms [8–11]. Other fractal-like geometries are found in nature suited to various functionalities, including spider capture silk for strength and elasticity [12], biological composites for stiffness and fracture toughness [13,14], and trabecular bone for stiffness and minimal weight [15]. Recently, novel manufacturing methods have allowed the principles of geometric hierarchy to be used in engineering design [16–19].

Structures that derive their mechanical properties predominantly from their geometry rather than their material composition are often referred to as "mechanical metamaterials" [20]. Use of geometry to control the mechanics of a system can lead to novel, beneficial properties, including auxetic response [21,22], energy trapping [23], mechanical cloaks [24], and high strength-to-weight ratios [25]. Here we look to control the mechanical response of a system made up of three materials by controlling the geometry of the structure; in particular, we investigate the effect of adding geometric hierarchy. It is widely observed that naturally occurring interfaces with nontrivial geometry exhibit remarkable mechanical properties [26–28]. Suture joints are a prime example of such geometric specialization for mechanical purposes, and such joints are typically observed joining two regions of a given material via an interfacial region comprising a second material with lower stiffness [28,29]. Examples of such joints are to be found in bone [2] (including the cranium [30]), turtle shell [29], and ammonites [14,31]. In all of these cases, mechanical function (including stiffness, strength, fracture resistance) is hypothesized to be a driving factor in the design of the interface; other functions for which such designs are specialized include growth, respiration, and buoyancy control [14,30,31]. While a range of geometries joining two domains of a given material with use of a second joining material (glue) have been extensively studied [2,7,14,26–31], the problem of joining two materials of

*daniel.rayneau.kirkhope@gmail.com

 © 2018 American Physical Society

differing stiffness has received little attention. This problem is of particular interest where dissimilar materials enable designs to achieve high structural efficiency in situations where stiffness, strength, and damage tolerance are all of relevance [32].

In this paper we focus on a novel application of hierarchical design—creating a permanent adhesive connection between two materials of differing stiffness. The geometry of both sides of the interface is designed to permit maximum interface stiffness and strength. The geometry we investigate is biologically inspired: we observe this particular geometry marking the transition from a stiff material to a softer material in equine and bovine hooves (Fig. 1). Here we investigate whether this form could be a specialization linked with mechanical function. One of the adaptations of the equine hoof observed at this junction is its hierarchical structure of laminae or lamellae [33,34]. Approximately 600 primary epidermal lamellae, each bearing 100–150 nonkeratinized secondary epidermal lamellae, increase the area for adhesion between the dermis and the epidermis to more than 2 m^2 [35]. Between the dermis and the epidermis is a set of biological molecules allowing tissues to remain bound together [36,37]. The geometry of this interface is assumed to be an anatomical specialization key to force mediation [38]. Clinical signs of laminitis (a disease causing lameness) occur when this hierarchical lamella architecture disintegrates [39], and thus natural-selection pressure should ensure a robust interface [40,41]. While the extensive surface area available for adhesion is used as justification for the ability of the equine hoof capsule to survive a large load [38,40,41], no studies have attempted to model this hypothesis. Given the widespread use of equids in developing countries [42–44] and the well-established economic cost of lameness in cattle [45,46], understanding laminitis would make great welfare and economic sense. Understanding the mechanical function of this biological interface is a critical step in alleviating diseases associated with its degradation.

In this paper we present a thorough investigation into the effect of hierarchical geometry on interface stiffness and stress distributions. Using analytic methods, confirmed through finite-element simulations, we demonstrate the dependence of scaling relationships defining interface stiffness on the hierarchical order of the geometry. We find stiffer interfaces are linked with increased hierarchy. In higher-order structures, we find that more than one scaling regime exists, and we present analytic arguments linking the different scaling regimes to specific deformation modes. Furthermore, we establish that hierarchical geometry leads to a reduced magnitude of stress observed in the material linking the two sides of the interface. On the basis of this observation, we make predictions about the region of the structure that will first exhibit nonelastic deformations and show this can be manipulated through alterations in the geometry of the interface.

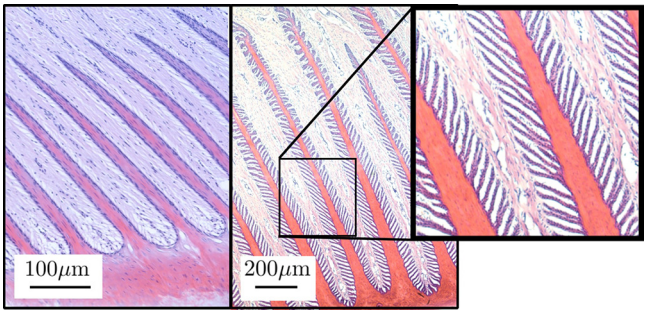

FIG. 1. A cross-section image taken perpendicular to the surface of the hoof wall. The image shows the interface between soft biological material and stiff keratinized materials found in the bovine (left) and equine (right) hoof. In both cases the hoof wall is situated below the region imaged, while the pedal bone is above the region imaged. This interface mediates large concussive loads between the two regions during animal locomotion. The secondary lamellae are on both the dermal and the epidermal lamellae and are clearly visible in the inset in the right-hand image.

II. GEOMETRY AND HIERARCHY

Here we focus on joining two materials of vastly differing stiffness via an intermediate elastic medium. We assume that the system is rectangular and that the upper region of the system is made up of only the stiffer material, while the lower region is made up of only the softer material. These two materials can be joined only via the intermediate material. As such, the three materials are referred to as "upper," "lower," and "intermediate," referring to their position in the composite (see Fig. 2). The upper material has stiffness much greater than the other materials in the structure and as such is modeled as infinitely stiff. The remaining two materials are both linear elastic, with Young's modulus and Poisson's ratio given by Y_i and ν_i for the intermediate material and Y_l and ν_l for the lower material. For a given system dimension, a pair of internal boundaries can then be defined specifying the geometry entirely: one boundary defines the transition from the lower to the intermediate material, and the second marks the transition from the intermediate to the upper material. The materials at each boundary are assumed to be perfectly bonded. A possible geometry showing the three material domains is shown in Fig. 2(a). We focus on geometries where the width of the intermediate domain is fixed. We therefore specify a single curve describing the center of the intermediate domain, and we require that the boundaries defining the geometry are a fixed distance $t_i/2$ from this curve; this width is measured in the direction normal to the tangent of the curve at that point.

The geometry investigated here can be described as being of varying "generation," each generation introducing a new length scale into the problem. The generation-0 geometry is shown in Fig. 2(a): the boundaries between

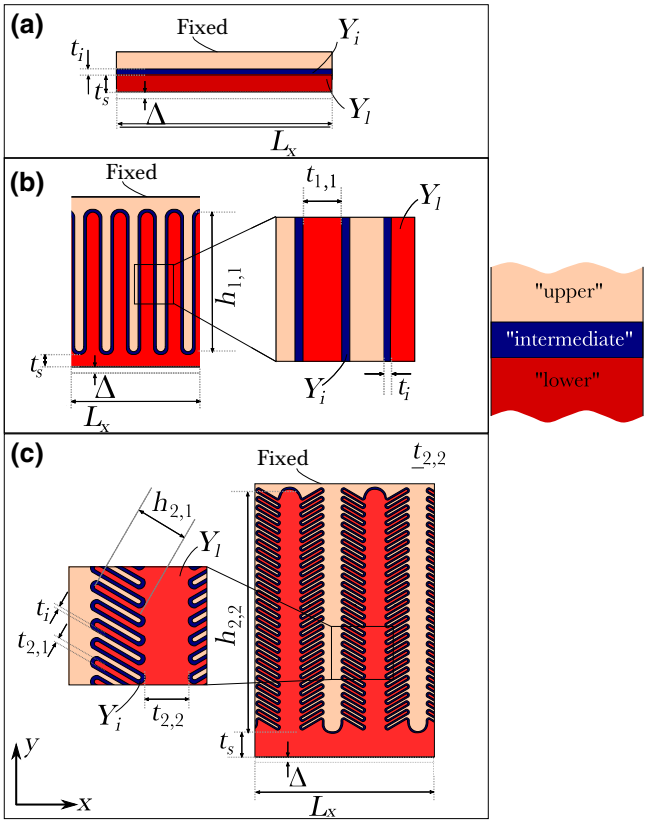

FIG. 2. (a) The generation-0 geometry: a planar connection of two materials of vastly differing stiffness joined by an adhesive connection of thickness t_i. (b) The generation-1 interface and its parameterization. (c) The generation-2 geometry: A pair of primary lamellae protrude from the deformable domain. From these primary lamellae, a secondary set of lamellae emanate at a given angle, θ ($\theta = \pi/3$ shown). The fixed domain interdigitates these deformable lamellae. In all three diagrams, the cream region represents an infinitely stiff material, which is connected to the deformable material (shown in red) via a (navy) intersurface interaction. An imposed displacement of Δ is applied to the lower surface of a given design, and the stiffness of the interface is evaluated.

the different materials form a pair of straight parallel lines. The generation-1 structure is designed such that the two materials to be joined (the upper and lower materials) form a set of interdigitating lamellae whose tips are rounded with semicircular caps. The lamellae introduced are both of equal length $h_{1,1}$ and thickness $t_{1,1}$; this geometry is shown in Fig. 2(b). To form the final geometry, we take the generation-1 structure and add a secondary set of interdigitating lamellae along the sides of the primary lamellae; this geometry is shown in Fig. 2(c). The angle at which the secondary lamellae protrude from the primary lamellae is set to be θ. We follow the notation used in similar work on hierarchical structures [18,19,25]: the parameter X describing the geometry on the ith length scale in a generation-G structure is denoted $X_{G,i}$, where $i = G$ is the longest length scale and $i = 1$ is the shortest (thus, for example, $t_{2,1}$ denotes the thickness of the secondary lamellae in a generation-2 structure). These geometries along with the notation used in their parameterization are shown in Fig. 2. An important variable governing the mechanics of these structures is the aspect ratio of the lamellae, and we define this as

$$a_{G,i} \equiv \frac{h_{G,i}}{t_{G,i}}. \tag{1}$$

When nonzero forces are applied to the upper and lower boundaries, a relative displacement between the two boundaries will be observed. Because of the infinite stiffness of the upper material, the relative displacement of these boundaries signifies deformation in the lower and intermediate materials only. We aim to investigate the effect of geometry, and in particular the addition of substructure, on the stiffness and strength of the interface.

III. RESULTS

Here we present the results of finite-element simulations calculating the stiffness of geometries with varying degrees of hierarchy along with analytic scaling results. The finite-element simulations are undertaken with the two-dimensional structural mechanics module of COMSOL MULTIPHYSICS 5.1 [47] with a plane-strain assumption. Mesh-refinement studies are undertaken to ascertain the accuracy of the results. For a given thickness of interface material, the required mesh density is highly dependent on the thickness of the lamellae in the geometry considered (further information on the finite-element simulations performed here can be found in the Appendix).

A. Stiffness

To test the stiffness of the interface, we fix the upper external boundary of the system and investigate the magnitude of the force that must be applied to the lower external boundary of the system to create a displacement of a given size and direction. The fixed boundaries in the geometries are labeled "fixed" in Fig. 2, and the displacement considered along the lower external boundary is indicated with a dashed gray line. We consider only small deformations such that the response of the structure is close to linear. We investigate structures being loaded under tension as this is the biologically relevant loading condition [48–50]. To find the stiffness of a given geometry under tension, we investigate what loading is required to create a deformation of magnitude Δ in the $-y$ direction relative to the upper boundary. We report the total loading resulting from the displacement of magnitude Δ and refer to it as a "reaction force" as it arises in response to the imposed displacement.

1. Generation 0

The generation-0 structure is composed of a planar interface between a deformable and an infinitely rigid material connected by an intermediate elastic medium; see Fig. 2. When a displacement is imposed on the base of the deformable surface (the lower external boundary of the system) relative to the infinitely stiff material, the nature of the deformation across the structure will be dependent on the stiffness of the intermediate material, Y_i, and that of the lower material, Y_l. The ratio of the stiffness is denoted η:

$$\eta = \frac{Y_l}{Y_i}. \tag{2}$$

We also introduce the nondimensional load parameter

$$f_R(G) \equiv \frac{F_R(G)}{Y_l \Delta}, \tag{3}$$

where Δ is the displacement imposed on the structure, G denotes the generation of the structure investigated, and F_R is the reaction load parallel to the imposed displacement per unit length in the remaining spatial dimension. For a fixed geometry and fixed Poisson's ratios, this parameterization collapses all pairs of (Y_i, Y_l) onto a single line. We can calculate $F_R(0)$ for $\eta \gg 1$ by noting that in this limit the system closely approximates two rigid bodies exerting a force on the intermediate layer. Thus, the reaction force for a given displacement is given by

$$F_R(0) = \frac{Y_i L_x}{t_i}\Delta. \tag{4}$$

From Eq. (3), we thus expect that for sufficiently large η, $f_R \sim \eta^{-1}$; this scaling is shown in Fig. 3 against results of finite-element simulations. This result is used as a benchmark for the more complex hierarchical geometries.

2. Generation 1

For the generation-1 and generation-2 designs, we introduce γ as the ratio of the total reaction force of the structure of interest to that of the generation-0 structure of the same width (L_x in Fig. 2) undergoing the same deformation:

$$\gamma \equiv \frac{f_R(G)}{f_R(0)}. \tag{5}$$

As shown in Fig. 2(a), the generation-1 geometry is made up of a flat interface between a deformable (with Young's modulus Y_l) and infinitely stiff material with a series of interdigitated lamellae protruding perpendicular to the interface from either side. The two materials are joined by an intermediate material with Young's modulus Y_i. The parameters used in obtaining the results given below are $t_{1,1} = 5 \times 10^{-4}$ m, $t_i = 1 \times 10^{-6}$ m, $t_s = 5 \times 10^{-5}$ m, $Y_i = 1 \times 10^8$ Pa, $\Delta = t_i/10$, and $\nu_l = \nu_i = 0.3$.

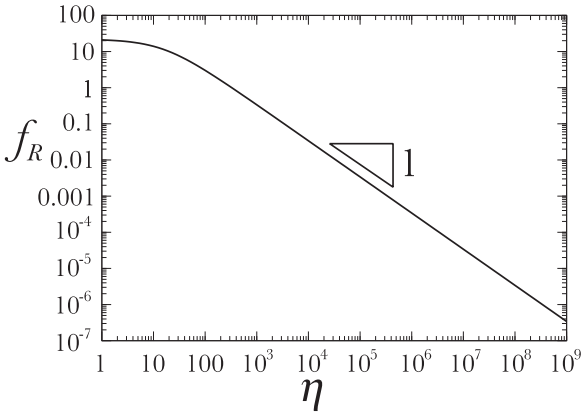

FIG. 3. The stiffness of a generation-0 interface. The reaction force shown is for a structure with parameters $L_x = 3 \times 10^{-4}$ m, $t_i = 1 \times 10^{-6}$ m, $Y_i = 100$ MPa, and $\Delta = t_i/10$.

We consider tension imposed on the deformable surface: a displacement in the $-y$ direction is imposed along the lower external boundary of the system, as indicated in Fig. 2, and the reaction force F_R on the structure is measured (see the Appendix). The maximum value of γ can be approximated through physical considerations. We can calculate the upper limit of $F_R(1)$ by noting that for $\eta \gg 1$ ($Y_l \gg Y_i$) the deformation in the structure will be limited to the intermediate material, and thus the system will approximate two infinitely stiff bodies joined by the intermediate material of stiffness Y_i [see the color map on the right in Fig. 4(b), the upper and lower material are displaced by uniform amounts]. Because of the geometry of the system, the response will be dominated by the region on the intermediate material that experiences shear loading. The force required to induce a displacement Δ across this material in shear is

$$F_R(1) = \frac{Y_i a_{1,1} t_{1,1}}{(1-\nu_i)t_i}\Delta. \tag{6}$$

Thus, in the limit of $\eta \gg 1$, the increase in stiffness compared with a generation-0 structure [Eq. (4)] is given by

$$\gamma = \frac{a_{1,1}}{2(1-\nu_i)}. \tag{7}$$

This expression is plotted in Fig. 4 along with the results of simulations. It is observed in Fig. 4(a) that before this plateau γ increases with increasing η. In this regime, the scaling of γ with η can be established through energy considerations: while γ is increasing with increasing η, it is observed that the tips of the lower set of lamellae are displaced less than the lamella base; the color map on the left in Fig. 4(b) shows a typical displacement in this regime. Most of the deformation within the structure is then limited to a region of the deformable materials close to the lamella base. We introduce the parameter $l^*_{G,i}$. This length

describes the distance from the base of the lamellae within which the structure experiences significant deformation. It is defined by an equivalence in energy stored in the deformation of the lamella structure and an isolated structure of length $l^\star_{G,i}$ with suitable boundary conditions experiencing uniform strain ($l^\star$ is not a quantity related to the geometry of the structure, but is a parameter that varies as a function of η, representing the extent to which the deformations penetrate into the interface structure). The strain energy stored in the lamella structure of the lower material scales in the same way as that of an isolated beam of width $t_{1,1}$ and length $l^\star_{1,1}$ fixed at one end and subject to a displacement Δ extending the structure parallel to its length:

$$U_l \sim \frac{Y_l t_{1,1}}{l^\star_{1,1}} \Delta^2. \tag{8}$$

The strain energy in deforming the intermediate material scales in the same manner as for an elastic material of length $l^\star_{1,1}$ subject to a shear displacement of magnitude Δ:

$$U_i \sim \frac{Y_i l^\star_{1,1}}{(1-\nu_i)t_i} \Delta^2. \tag{9}$$

Selecting the value of $l^\star_{1,1}$ that minimizes the internal energy $(U_i + U_l)$ in the system, assuming nonzero displacement Δ, we find the scaling $l^\star_{1,1} \sim \eta^{1/2}$. Using Eqs. (4), (5), and (7), for fixed $t_{1,1}$, we see that in this regime

$$\gamma \sim \eta^{1/2}. \tag{10}$$

This scaling is plotted in Fig. 4 along with the results of finite-element simulations.

Fitting the results of finite-element simulations within an appropriate range of η gives a scaling of $\gamma \sim \eta^{0.50}$, where the error in the power is ± 0.01.

3. Generation 2

Here we establish the mechanical response of the generation-2 structure when the lower external boundary is displaced under tension. In this structure, the lower material makes up two sets of lamellae: the primary lamellae of length $h_{2,2}$ and thickness $t_{2,2}$ and the secondary lamellae of length $h_{2,1}$ and thickness $t_{2,1}$. We perform finite-element simulations on structures whose primary and secondary lamellae have a range of aspect ratios between 4 and 64; the effect of other parameters can be elucidated from the analytic work presented below. The parameters used in the simulations presented here are $h_{2,1} = 8 \times 10^{-5}$ m, $t_{2,2} = 5 \times 10^{-4}$ m, $t_i = 10^{-6}$ m, $t_s = 5 \times 10^{-5}$ m, $Y_i = 10^8$ Pa, $\Delta = t_i/10$, and $\nu_l = \nu_i = 0.3$. Other geometric and material parameters are given by a specific aspect ratio and η value.

We analyze the response of the structure when a displacement in the $-y$ direction is imposed on the lower external boundary, as indicated in Fig. 2. In the limit of large η ($Y_i \ll Y_l$), any displacement imposed on the external boundary of the lower material will indicate a deformation in the intermediate material. A typical deformation in this regime is shown in the color map on the right in Fig. 5(b), where the lower material shows a uniform displacement. The force required to impose a given displacement in this limit can be approximated as

$$F_2 = \frac{4h_{2,2}h_{2,1}Y_i}{2t_i t_{2,1}}. \tag{11}$$

With Eq. (4), the maximum value of γ can then be calculated; this maximum value is indicated in Fig. 5(a) for $a_{2,2} = 4$. For small $a_{2,2}$ and large $a_{2,1}$, we observe a scaling

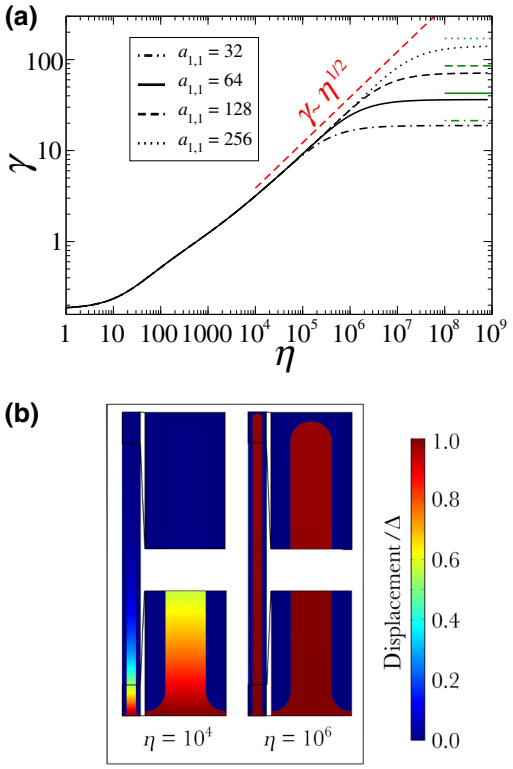

FIG. 4. (a) The stiffness increase of a generation-1 interface relative to a flat geometry (generation 0) as a function of η. The interface is loaded under tension and the stiffness of the interface is measured (see the Appendix). Also shown are the results for various aspect ratios of the structure, $a_{1,1}$, as defined in Eq. (1). The maximum values of γ as predicted by Eq. (7) are shown by green lines. The results of the simulations get closer to these predicted values in the limit of large η. The scaling of $\gamma \sim \eta^{1/2}$ is shown in red; this scaling is predicted by Eq. (10). (b) Color maps indicating the magnitude of the displacement of the lamella ($a_{1,1} = 32$); for $\eta = 10^4$ close to zero displacement is observed at the tip of the lamella structure, while for $\eta = 10^6$, the whole lamella approximates a rigid body and thus the value of γ plateaus. For both color maps, the parameters used are described in the main text.

law immediately before γ reaches its plateau. We hypothesize that this scaling law is observed when the primary lamellae in the structure closely resemble rigid bodies, and the secondary lamellae experience a deformation within a distance $l^{\star}_{2,1}$ of their connection with the primary lamellae; a snapshot from a simulation showing typical deformation in this regime is shown in the middle in Fig. 5(b). We support this hypothesis with a scaling argument: in this regime the secondary lamellae will bend, and the energy associated with this slender structure of length $l^{\star}_{2,1}$ and thickness $t_{2,1}$ bending with a displacement Δ at its tip scales as

$$U_l \sim \frac{Y_l l^3_{2,1}}{l^{\star 3}_{2,1}} \Delta^2. \tag{12}$$

The strain energy in the interface will scale as a tension/compression strain of magnitude Δ/t_i imposed over a region of length $l^{\star}_{2,1}$; thus,

$$U_i \sim \frac{Y_i l^{\star}_{2,1}}{t_i} \Delta^2. \tag{13}$$

Selecting the value of $l^{\star}_{2,1}$ so as to minimize the internal energy of deformation (assuming nonzero Δ), we find that $l^{\star}_{2,1} \sim \eta^{1/4}$. Given the force the structure will support will be proportional to the area over which strain is spread [Eq. (11)], we see that in this regime

$$\gamma \sim \eta^{1/4}. \tag{14}$$

For sufficiently large values of $a_{2,2}$ and $a_{2,1}$, before the $\gamma \sim \eta^{1/4}$ regime we observe a second scaling law. In this regime both the primary and the secondary lamellae will deform within a characteristic length, $l^{\star}_{2,2}$ and $l^{\star}_{2,1}$, respectively (where $l^{\star}_{2,2} < h_{2,2}$ and $l^{\star}_{2,1} < h_{2,1}$). Increasing η will serve to increase $l^{\star}_{2,1}$ and $l^{\star}_{2,2}$. The scaling of $l^{\star}_{2,2}$ can be calculated by consideration of the energy of deformation of both the lower material and the intermediate material; these are given by

$$U_l \sim Y_s \left(\frac{t_{2,2}}{l^{\star}_{2,2}} + \frac{t_{2,1} l^{\star}_{2,2}}{l^{\star}_{2,1} t_{2,1}} \right) \Delta^2, \quad U_i \sim \frac{Y_i l^{\star}_{2,1} l^{\star}_{2,2}}{t_i t_{2,1}} \Delta^2. \tag{15}$$

The expression for U_l is made up of two terms: the stretching of the primary lamellae (first term) and the bending of the secondary lamellae (second term). Selecting the value of $l^{\star}_{2,2}$ that minimizes the total energy of the system (for a nonzero displacement Δ), noting that $l^{\star}_{2,1} \sim \eta^{1/4}$, we see that for $\eta \gg 1$, $l^{\star}_{2,2} \sim \eta^{3/8}$. Thus, from Eqs. (4), (5), and (11), we see that in this regime

$$\gamma \sim \eta^{5/8}. \tag{16}$$

These scaling laws are shown in Fig. 5 along with the results of finite-element simulations.

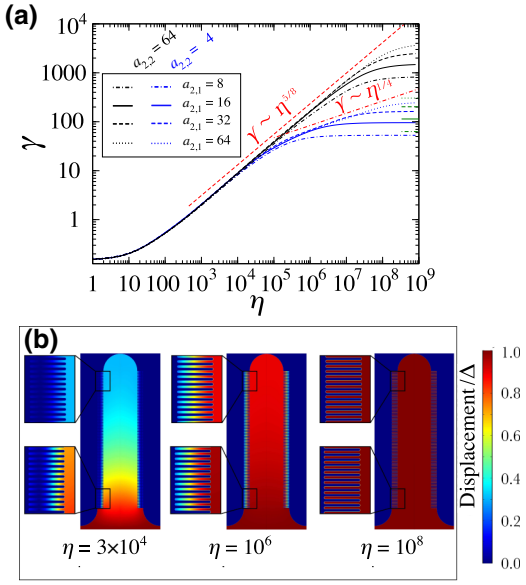

FIG. 5. (a) The stiffness increase of a generation-2 interface relative to a generation-0 geometry for various values of the aspect ratio. The interface is loaded under tension and the stiffness of the interface is measured. The results are shown for various structures where the aspect ratio of both the primary and the secondary lamellae ($a_{2,2}$ and $a_{2,1}$, respectively) are varied. (b) Snapshots of simulations showing the displacement on the lamella structure for various η with $a_{2,2} = 4$, $a_{2,1} = 16$: $\eta = 3 \times 10^3$ is in the regime whereby increasing η serves to increase displacement toward the tips of the primary and secondary lamellae; at $\eta = 10^6$ the primary lamella acts similarly to a rigid body (the displacement at the tip of the lamella is more than 90% of that at the base), and increasing η serves primarily to increase the displacement toward the tip of the secondary lamellae; for $\eta = 10^8$ all lamella structures move as rigid bodies, and almost all strain is observed in the intermediate material. These three snapshots are from the regimes of $\gamma \sim \eta^{5/8}$, $\gamma \sim \eta^{1/4}$, and γ independent of η, respectively.

B. Stress distribution and hierarchy

In this section we investigate the stress distributions present within the hierarchical lamella structures to further elucidate the mechanics of the system. First, we establish the nature of the stresses within the primary lamellae as a function of the distance from the lamella base. We then show the dependence of the maximum von Mises stress within the structure on the interface geometry. Finally, we make a hypothesis on the region in which failure is likely to start for various geometries.

We first examine the magnitude of the σ_{yy} component of stress down the center of the primary lamellae in the generation-1 and generation-2 structures. We find that for both the generation-1 and the generation-2 structures, the magnitude of the stress decreases exponentially as a function of distance from the lamella base s; that is, $|\sigma_{yy}| \sim \exp(-ks)$ [see Fig. 6(a)]. For a given geometry, k varies

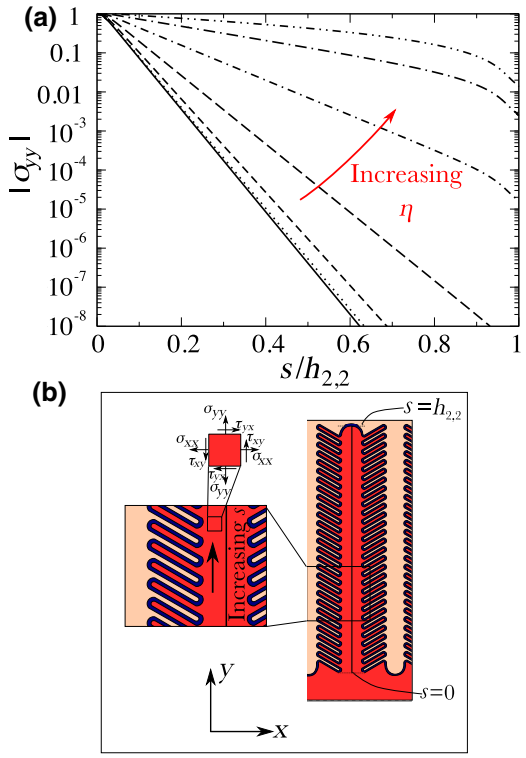

FIG. 6. (a) Semilog plot of σ_{yy} down the center of the primary lamella as a function of the distance from the lamella base for a particular structure ($a_{2,2} = 16$, $a_{2,1} = 4$ with all other dimensions as given in the Sec. III A 3), for values of $\eta = 10^n$ with integer n from 0 to 7. An exponential decay in the magnitude of the stress for η smaller than that taken for γ to plateau (see Fig. 5) is observed. (b) The region in which σ_{yy} is evaluated.

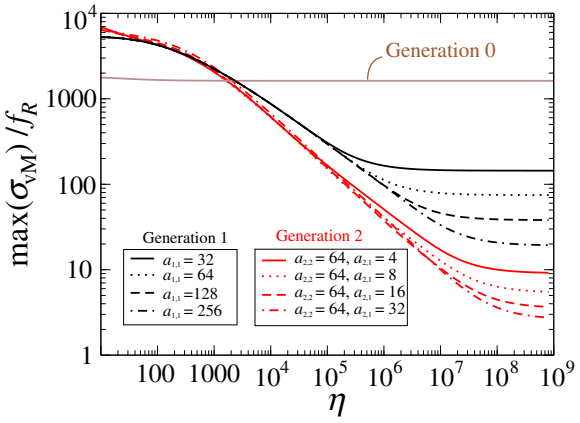

FIG. 7. The maximum von Mises stress observed in the interface material, scaled by the total reaction force on the boundary of a set of generation-0, generation-1, and generation-2 structures. For η greater than 10^3, hierarchical structures better protect the interface material from high-magnitude stresses and generation-2 structures outperform the generation-1 structures.

as a function of η, the relative stiffness of the intermediate and lower materials. For sufficiently large η, the decay is no longer exponential, and this coincides with γ reaching its plateau value.

In Fig. 7, we present the maximum value of the von Mises stress ($\sigma_{\mathrm{vM}} = \sqrt{\sigma_{xx}^2 + \sigma_{yy}^2 - \sigma_{xx}\sigma_{yy} + 3\tau_{xy}^2}$) present within the intermediate material, scaled by the reaction force at the boundary where the displacement is imposed. This measure gives an indication of how effective the geometry is at creating a strong adhesive connection utilizing a weak connective material. For η greater than approximately 10^3, hierarchical geometries provide an advantage in terms of withstanding loading for a given intermediate-material stress. The generation-2 structure investigated here provides advantages over the generation-1 structure for η larger than approximately 10^3.

Finally, we look at the expected failure region of the structure and the effect of hierarchy. The structure considered here is made of two deformable materials: an intermediate material and a lower material (navy and red in Fig. 2). These two materials can be assigned a yield stress, σ_{Y_1} and σ_{Y_2} for the intermediate material and the lower material, respectively. When the structure is loaded, either material can initiate plastic deformation. This will occur when the maximum von Mises stress exceeds the yield stress of the material. For a given geometry, the region in which nonelastic deformation first occurs depends on the value of η considered and the $\sigma_{Y_1}/\sigma_{Y_2}$ ratio. To establish the region that will exhibit nonelastic deformation first, we use the following procedure: Impose a displacement on the lower external boundary of the structure in the $-y$ direction (as in the investigations into stiffness); then establish the maximum von Mises stress in the two deformable domains; assuming nonelastic deformations occur before large geometric nonlinearities are observed, the ratio of these maximum stresses indicates the ratio of σ_{Y_1} to σ_{Y_2} for which the region of failure transitions from the interface to the lamallae. The space $(\eta, \sigma_{Y_1}/\sigma_{Y_2})$ can then be split into the two regions shown in Fig. 8. For low values of η and a low $\sigma_{Y_1}/\sigma_{Y_2}$ ratio, we see the intermediate material will fail first for both generation-1 and generation-2 structures, while for sufficiently high values of η and high $\sigma_{Y_1}/\sigma_{Y_2}$ ratios, plastic deformation in the lower material will occur first.

IV. SUMMARY

We show that a geometry based on that observed in the equine hoof is conducive to a stiff interface between two materials of vastly differing stiffness. We demonstrate that through increase of the number of length scales within the structure, the scaling laws relating the stiffness of the constituent materials to the global interface stiffness can be manipulated in a systematic manner. We link these different scaling regimes with different deformation modes within the structure and support these hypotheses

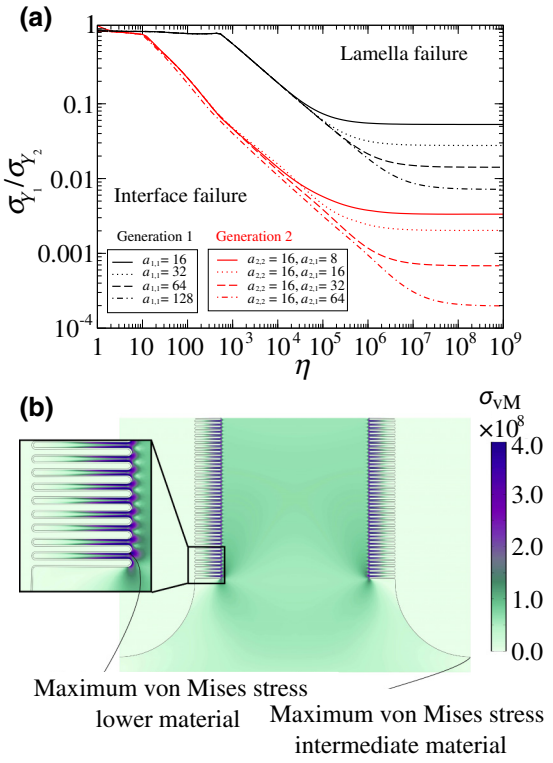

FIG. 8. (a) The expected region of failure in the structure connecting two different materials. Above the curve describing a given geometry, the material making up the lamella structure will experience nonelastic deformation before the interface material, and the reverse occurs below the curve. (b) The location of the maximum stresses in a particular generation-2 structure, where the colour map indicates the magnitude of the von Mises stress at that point.

with scaling-law arguments. Furthermore, by altering the aspect ratio of the lamellae, we find the value of η at the transition from one scaling regime to another can be manipulated.

We show that the hierarchical geometry leads to a reduced maximum stress observed in the intermediate material for a given magnitude of loading. Furthermore, we demonstrate that the ratio of maximum stresses in the intermediate material to those in the lamellae can be manipulated over orders of magnitude through alterations in the geometry of the structure. These findings are of particular relevance given the recent growth of digital manufacturing techniques that allow the fabrication of two-dimensional structures with features on the nano or micro length scale [51]. In many areas of application, the materials to be joined may be specified by the functionality of the desired structure, and thus η is set by the application. For a given η, we show that through close control of geometry, it is possible to create interfaces with high stiffness, a selectable failure mode, and tailorable stresses within the interface material. This method thus allows enhanced functionality of structures by permitting a less-restricted choice of constituent materials.

In principle, higher-generation structures could be created by addition of further substructure to the generation-2 geometry proposed here. It is hypothesized that the addition of extra substructures would further alter the scaling relationships established here, and it is thought that such a structure would exhibit trends similar to those observed in other hierarchical metamaterials whereby the scaling tends toward a well-defined limit [25]. Although this work shows the tailorability of interface stiffness through hierarchy, open questions remain regarding the fracture properties, ductility, and strength of these intricate architectures.

This work highlights the general importance of geometry in the creation of joints between dissimilar materials, allowing composite and hybrid structures with enhanced structural efficiency [32]. A natural application for this composite joint is to be found in medical implants where high-performance joints between dissimilar materials are of key importance. Here the tailorability of the resultant joint and the use of an intermediate material that experiences minimal mechanical stresses is of great practical importance as it permits the reduction of stress concentrations and greater biocompatibility [32]. Our work also offers a new perspective on the development of tendon-bone interfaces, where the low success rates of graft implantation along with the increased occurrence of musculoskeletal injuries necessitate the development of novel repair strategies [52]. Furthermore, it is widely observed that natural composites simultaneously exhibit high stiffness and fracture resistance [13,14], and it is hypothesized here that by designing the interface between the different constituent materials, one can obtain metamaterials that match or exceed the performance of their naturally occurring analogs.

Not only does this work have implications for the design of geometry in the engineering challenge of joining two materials of differing stiffness, it also lends credence to the long-assumed role of hierarchical interface geometry in the equine hoof: such geometry has been selected by evolutionary pressures (among other reasons) for a mechanical purpose. Despite the undoubted complexity of the biological system, it is expected that the main findings of this work will apply to the interface observed within the hoof: increasing the hierarchy of the interface serves to increase the mechanical stiffness of the interface (this is also notable for the previously reported link between stiffness and strength of composite structures—it is widely observed that the presence of one implies the presence of the other [53]). We believe that with more theoretical analysis of hierarchical structures, together with increased ability to fabricate these intricate architectures, hierarchical architectures will become more widely used in engineering designs of the future.

ACKNOWLEDGMENTS

The authors thank Catrin Rutland, David Neal, and Ramzi Al-Agele for insightful conversations regarding the presented work. D.R.-K. acknowledges funding support from the Academy of Finland and thanks Giulio Costantini for useful discussions regarding the manuscript. C.R. acknowledges funding support from Petplan Charitable Trust and Waltham Centre for Pet Nutrition.

APPENDIX: METHODS

All simulations presented in this work are undertaken with the solid mechanics module of COMSOL MULTIPHYSICS 5.1 performing "stationary" (quasistatic) studies. The geometry is made up of three materials, as shown in Fig. 2. The upper material is modeled as infinitely stiff (with use of the built-in "rigid domain" option of COMSOL MULTIPHYSICS). The remaining two materials are linear elastic and are described by the parameters given in the main text. Meshing is performed with the built-in COMSOL MULTIPHYSICS routines. Mesh-refinement studies are performed to establish the accuracy of the results (checking for convergence of results). The upper external boundary is then fixed in space, while the lower external boundary has a displacement imposed on it in the $-y$ direction, as shown in Fig. 2. The equilibrium position of the structure is then obtained, and the reaction force on the lower boundary is evaluated through integration (built-in COMSOL MULTIPHYSICS routine). This reaction force is equivalent to the force that would be required to induce the displacement considered.

[1] W. Federle, Why are so many adhesive pads hairy? J. Exp. Biol. **209**, 2611 (2006).

[2] H. Yao and H. Gao, Mechanics of robust and releasable adhesion in biology: Bottomup designed hierarchical structures of gecko, J. Mech. Phys. Solids **54**, 1120 (2006).

[3] D. Labontea, C. J. Clemente, A. Dittrich, C.-Y. Kuo, A. J. Crosby, D. J. Irschick, and W. Federle, Extreme positive allometry of animal adhesive pads and the size limits of adhesion-based climbing, Proc. Natl Acad. Sci. **113**, 1297 (2016).

[4] G. Huber, H. Mantz, R. Spolenak, K. Mecke, K. Jacobs, S. N. Gorb, and E. Arzt, Evidence for capillarity contributions to gecko adhesion from single spatula nanomechanical measurements, Proc. Natl Acad. Sci. **102**, 16293 (2005).

[5] W. J. Stewart and T. E. Higham, Passively stuck: Death does not affect gecko adhesion strength, Bio. Lett. **10**, 20140701 (2014).

[6] K. Autumn, M. Sitti, Y. A. Liang, A. M. Peattie, W. R. Hansen, S. Sponberg, T. W. Kenny, R. Fearing, J. N. Israelachvili, and R. J. Full, Evidence for van der Waals adhesion in gecko setae, Proc. Natl Acad. Sci. **99**, 12252 (2002).

[7] H. Yao and H. Gao, in *Structural Interfaces and Attachments in Biology*, Edited by S. Thomopoulos, S. Birmanx, and G. Genin (Springer, New York, 2013).

[8] M. R. Cutkosky, Climbing with adhesion: From bioinspiration to biounderstanding, Interface Focus **5**, 20150015 (2015).

[9] A. K. Geim, S. V. Dubonos, I. V. Grigorieva, K. S. Novoselov, A. A. Zhukov, and S. Yu Shapoval, Microfabricated adhesive mimicking gecko foot-hair, Nat. Mat. **2**, 461 (2003).

[10] D. Brodoceanu, C. T. Bauer, E. Kroner, E. Arzt, and T. Kraus, Hierarchical bioinspired adhesive surfacesa review, Bioinspir. Biomim. **11**, 051001 (2016).

[11] K. Autumn and N. Gravish, Gecko adhesion: Evolutionary nanotechnology, Phil. Trans. R. Soc. A **366**, 1575 (2008).

[12] H. Zhou and Y. Zhang, Hierarchical Chain Model of Spider Capture Silk Elasticity, Phys. Rev. Lett. **94**, 028104 (2005).

[13] R. O. Ritchie, The conflicts between strength and toughness, Nat. Mater. **10**, 817 (2011).

[14] Y. Li, C. Ortiz, and M. C. Boyce, Bioinspired, mechanical, deterministic fractal model for hierarchical suture joints, Phys. Rev. E. **85**, 031901 (2012).

[15] R. Huiskes, R. Ruimerman, G. H. van Lenthe, and J. D. Janssen, Effects of mechanical forces on maintenance and adaptation of form in trabecular bone, Nature **405**, 704 (2000).

[16] T. A. Schaelder, A. J. Jacobsen, A. Torrents, A. E. Sorensen, J. Lian, J. R. Greer, L. Valdevit, and W. B. Carter, Ultralight metallic microlattices, Science **334**, 962 (2011).

[17] E. Lin, Y. Li, J. C. Weaver, C. Ortiz, and M. C. Boyce, Tunability and enhancement of mechanical behavior with additively manufactured bio-inspired hierarchical suture interfaces, J. Mat. Res. **9**, 1867 (2014).

[18] D. Rayneau-Kirkhope, Y. Mao, and R. S. Farr, Optimization of fractal space frames under gentle compressive load, Phys. Rev. E. **87**, 063204 (2013).

[19] D. Rayneau-Kirkhope, Y. Mao, and R. S. Farr, Ultralight Fractal Structures from Hollow Tubes, Phys. Rev. Lett. **109**, 204301 (2012).

[20] P. Reis, H. Jaeger, and M. van Hecke, Designer matter: A perspective, Ext. Mech. Lett. **5**, 25 (2015).

[21] T. Mullin, W. Deschanel, K. Bertoldi, and M. C. Boyce, Pattern Transformation Triggered by Deformation, Phys. Rev. Lett. **99**, 084301 (2007).

[22] K. Bertoldi, P. M. Reis, S. Willshaw, and T. Mullin, Negative Poisson's ratio behavior induced by an elastic instability, Adv. Mater. **22**, 361 (2010).

[23] B. Florijn, C. Coulais, and M. van Hecke, Programmable Mechanical Metamaterials, Phys. Rev. Lett. **113**, 175503 (2014).

[24] T. Buckmann, M. Kadic, R. Schittny, and M. Wegener, Mechanical cloak design by direct lattice transformation, Proc. Natl Acad. Sci. **112**, 4930 (2015).

[25] D. Rayneau-Kirkhope, Y. Mao, and R. S. Farr, Ultra-light hierarchical meta-materials on a body-centred cubic lattice, EPL **119**, 14001 (2017).

[26] E. Lin, Y. Li, C. Ortiz, and M. C. Boyce, 3D printed, bioinspired prototypes and analytical models for structured suture interfaces with geometrically-tuned deformation and failure behavior, J. Mech. Phys. Solids **73**, 166 (2014).

[27] Y. Li, C. Ortiz, and M. C. Boyce, Stiffness and strength of suture joints in nature, Phys. Rev. E. **84**, 062904 (2012).
[28] Y. Li, C. Ortiz, and M. C. Boyce, A generalized mechanical model for suture interfaces of arbitrary geometry, J. Mech. Phys. Solids **61**, 1144 (2013).
[29] S. Krauss, E. Monsonego-Ornan, E. Zelzer, P. Fratzl, and R. Shahar, Mechanical function of a complex three-dimensional suture joining the bony elements in the shell of the red-eared slider turtle, Adv. Mat. **21**, 407 (2009).
[30] R. P. Hubbard, J. W. Melvin, and I. T. Barodawala, Flexure of cranial sutures, J. Biomech. **4**, 491 (1971).
[31] S. Inoue and S. Kondo, Suture pattern formation in ammonites and the unknown rear mantle structure, Sci. Rep. **6**, 33689 (2016).
[32] R. W. Messler, Jr., *Joining of Materials and Structures: From Pragmatic Process to Enabling Technology* (Elsevier Butterworth-Heinemann, Burlington, 2004).
[33] J. E. Stump, Anatomy of the normal equine foot, including microscopic features of the laminar region, J. Am. Vet. Med. Assoc. **151**, 1588 (1967).
[34] R. A. Kainer, Clinical anatomy of the equine foot, Vet. Clin. North Am. Equine Pract. **5**, 271 (1989).
[35] C. C. Pollitt, The anatomy and physiology of the hoof wall, Equine Vet. Educ. **10**, 318 (1998).
[36] M. G. Farquhar and G. E. Palade, Junctional complexes in various epithelia, J. Cell Biol. **17**, 375 (1963).
[37] C. Rauch and M. Cherkaoui-Rbati, Physics of nail conditions: Why do ingrown nails always happen in the big toes? Phys. Biol. **11**, 066004 (2014).
[38] C. C. Pollitt, The anatomy and physiology of the hoof wall, Equine Vet. Educ. **10**, 318 (1996).
[39] C. C. Pollitt, Equine laminitis: A revised pathophysiology, AAEP Proc. **45**, 188 (1999).
[40] C. C. Pollitt, Anatomy and physiology of the inner hoof wall, Clin. Tech. Equine Pract. **3**, 3 (2004).
[41] C. C. Pollitt, Laminitic pain: Parallels with pain states in humans and other species, Vet. Clin. North Am. Equine Pract. **26**, 643 (2010).
[42] J. C. Pritchard, A. C. Lindberg, D. C. Main, and H. R. Whay, Assessment of the welfare of working horses, mules and donkeys, using health and behaviour parameters, Prev. Vet. Med. **69**, 265 (2005).
[43] A. Doumbia, in *Society for the Protection of Animals Abroad, the 7th International Colloquium on Working Equids, London, UK, 2014*.
[44] J. Pritchard, M. Upjohn, and T. Hirson, Improving working equine welfare in 'hard-win' situations, where gains are difficult, expensive or marginal, PLoS One **13**, e0191950 (2018).
[45] J. J. Vermunt, "Subclinical" laminitis in dairy cattle, N. Z. Vet. J. **40**, 133 (1992).
[46] C. Lischer and P. Ossent, Laminitis in cattle: A literature review, Tierarztl Prax **22**, 424 (1994).
[47] COMSOL Inc., http://www.comsol.com/comsol-multiphysics
[48] J. E. Douglas and J. J. Thomason, Shape, orientation and spacing of the primary epidermal laminae in the hooves of neonatal and adult horses (Equus caballus), Cells Tissues Organs **166**, 304 (2000).
[49] B. Faramarzi, Morphological spectrum of primary epidermal laminae in the forehoof of Thoroughbred horses, Equine Vet. J. **43**, 732 (2011).
[50] J. J. Thomason, J. E. Douglas, and W. Sears, Morphology of the laminar junction in relation to the shape of the hoof capsule and distal phalanx in adult horses (Equus caballus), Cells Tissues Organs **168**, 295 (2001).
[51] J. Valente, E. Plum, I. Youngs, and N. Zheludev, Nano- and micro-auxetic plasmonic materials, Adv. Mat. **28**, 5176 (2016).
[52] J. Z. Paxton, K. Baar, and L. M. Grover, Current progress in enthesis repair: Strategies for interfacial tissue engineering, Orthop. Muscular Syst. **S1**, 1 (2012).
[53] F. Barthelat and M. Mirkhalaf, The quest for stiff, strong and tough hybrid materials: An exhaustive exploration, J. R. Soc. Interface **10**, 20130711 (2013).